THE ASTROPHYSICAL JOURNAL, 285:312–321, 1984 October 1

ON THE EXCITATION OF CH MICROWAVE LINES

V. BUJARRABAL,[1] I. GONZALO,[2] AND F. SALINAS[1]

Received 1983 July 14; accepted 1984 March 9

ABSTRACT

Along with the very frequent occurrence of every CH 9 cm line inversion, CH radio observations also show the existence of another almost universal characteristic of this line's excitation: the overexcitation of the satellite $F = 0 \rightarrow 1$ line. Attempts to explain this fact, by means of quite a wide sample of local and nonlocal models as presented here, failed when line overlap was not taken into account.

As will be shown, the overlap of two components ($F = 2^+ \rightarrow 1^-$ and $F = 1^+ \rightarrow 1^-$) of the $^2\Pi_{1/2}$ $J = 3/2 \rightarrow J = 1/2$ rotational transition leads to the above-mentioned satellite-line anomalies. The numerical results are in reasonable agreement with the observations, and the mechanism satisfies the requirement of universality.

Subject headings: interstellar: molecules — molecular processes

I. INTRODUCTION

The CH 9 cm lines present favorable conditions for observation, and quite a complete set of experimental data from these lines in the interstellar medium exists today.

A primary analysis of the bulk of these observations immediately suggests the two main features of the interstellar CH excitation: the inversion of all three lines in the majority of the sources and a strong asymmetry between the hyperfine components, consisting of a net overexcitation of the $F = 0 \rightarrow 1$ transition. Figure 1 shows rotational energy levels of CH. Parity, total angular momentum J (without nuclear spin I), $F(\boldsymbol{F} = \boldsymbol{J} + \boldsymbol{I})$, and the 9 cm transitions have been indicated.

The inversion of the 9 cm lines seems to be very generalized, as is indicated by the fact that they are very often observed in emission, even in front of strong continuum sources such as Cas A and Ori A. This quite ubiquitous feature has been satisfactorily explained as a result of a parity discrimination in the collisional transition rates between the rotational ground state and the first excited state, $^2\Pi_{1/2}$ $J = 3/2$ (see Bertojo, Cheung, and Townes 1976; Elitzur 1977; Dixon and Field 1979*a*, *b*; the collisional law is also discussed in § II). The inversion mechanism is very simple, the $+ \rightarrow +$ collisions are more probable than the $- \rightarrow -$ ones, and then the subsequent radiative cascade ($- \rightarrow +$, $+ \rightarrow -$) tends to overpopulate the upper ($-$) level of the $^2\Pi_{1/2}$ $J = 1/2$ state with respect to the lower ($+$) level. At kinetic temperatures high enough to make this collisional pumping possible, the result is an inversion of the ground-state transitions.

The hyperfine asymmetry appears clearly when a cloud can be observed both in front of a continuum source and also beside it, just against the 2.7 background (ON-OFF experiments). The simplest model for these measurements will be considered. The OFF continuum source brightness temperature is given by

$$F_{B_{\rm OFF}} = (T_{\rm ex} - T_{\rm BG})[1 - \exp(-\tau)] \approx (T_{\rm ex} - T_{\rm BG})\tau$$
$$\propto (T_{\rm ex} - T_{\rm BG}) f N_{\rm CH}/T_{\rm ex} \approx f N_{\rm CH}$$

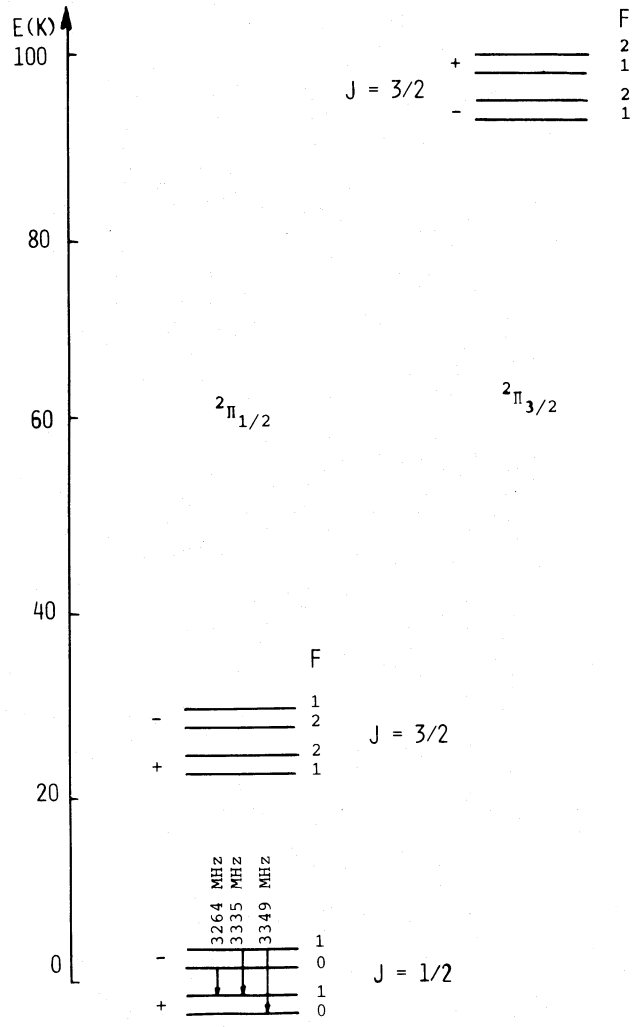

FIG. 1.—Lowest hyperfine levels of CH; only the excited states radiatively connected with the ground level are represented. Splittings are not to scale.

[1] Observatorio Astronómico Nacional, Centro Astronómico de Yebes, Apartado 148, Guadalajara, Spain.

[2] Departamento de Optica y Estructura de la Materia, Facultad de Ciencias Fisicas, Universidad Complutense, Madrid, Spain.

(f is the line strength, T_{ex} the excitation temperature, and N_{CH} the column density). The ON brightness temperature is

$$T_{B_{ON}} = (T_{ex} - T_C)[1 - \exp(-\tau)] \approx (T_{ex} - T_C)\tau$$
$$\propto (T_{ex} - T_C) f N_{CH}/T_{ex} \approx -T_C f N_{CH}/T_{ex}$$

(T_C is the continuum brightness temperature).

For observations just in front of the cosmic background ($T_{BG} = 2.7$ K), the line intensities have approximately the theoretical ratio

$$0 \rightarrow 1/1 \rightarrow 1/1 \rightarrow 0 = 1/2/1$$

(as can be generally observed), which is independent of the exact state of excitation of the lines. However, for the ON measurements, the observational intensity is approximately proportional to f/T_{ex}, and differences in excitation are now manifest.

The observations are conclusive: In the Ori A region, the $0 \rightarrow 1$ and the $1 \rightarrow 1$ lines have almost the same intensity in front of the continuum source. However, beside it, only the $1 \rightarrow 1$ transition is frequently detected. In W3C2 the three lines are nearly in the theoretical ratio outside the source, but the $0 \rightarrow 1$ is 2 times stronger than the others in front of it. Against the continuum of W43, the $0 \rightarrow 1$ line is just as intense as 0.25 K, whereas the others are hardly detected to a noise of 0.03 K (Rydbeck *et al.* 1976). Even in the sources in which the two other lines are observed in absorption (M17, RCW 38, G327.3−0.5, NGC 6334), the $0 \rightarrow 1$ line is always observed in emission. Thus, it can be said that all the observations confirm the $0 \rightarrow 1$ overexcitation, or, at least, that they are consistent with it.

Even though some explanations have been suggested, no detailed investigation of the mechanism responsible for this important feature has been presented to date.

A selectivity in collisional rates between hyperfine levels could induce differences in the excitation of the 9 cm line components. However, this possibility implies conjectures about rather unknown parameters. Also it presents difficulties in another characteristic, which arises in a more detailed analysis of the data: the fact that the excitation of the $1 \rightarrow 0$ transition is generally higher and not lower than that of the $1 \rightarrow 1$ transition. This point will be briefly discussed in §§ II and III*a*.

Anomalies in the satellite lines can be found in the presence of trapping in the two $J = 3/2 \rightarrow J = 1/2$ rotational transitions. In the first-order treatment, however, it induces underexcitation not overexcitation of the $0 \rightarrow 1$ transition. The mechanism is very similar to that explained by Elitzur (1976) for inversion of the OH $F = 2 \rightarrow 1$ transition (see § III). The trapping in the components of the radiative cascade from the $^2\Pi_{1/2}$ $J = 3/2$ or $^2\Pi_{3/2}$ $J = 3/2$ states to the ground state modifies their probabilities (originally equal to the Einstein A-coefficients), which become inversely proportional to the degeneration of the upper hyperfine levels. Cascades tend in this case to overpopulate the $F = 1$ ground levels and therefore to diminish (enhance) the excitation of the $0 \rightarrow 1$ ($1 \rightarrow 0$) transition. The main difference between OH and CH is that for this latter molecule, only two rotational excited states ($^2\Pi_{1/2}$ $J = 3/2$, $^2\Pi_{3/2}$ $J = 3/2$) are radiatively connected to the ground state. For both of them, trapping behaves in the same way, i.e., leading a situation evidently contradictory to that experienced.

Along with pointing out the importance and nature of the differences in excitation between the CH 9 cm components, the purpose of this paper is to find a convincing explanation for the origin of these anomalies.

II. COLLISIONAL RATES

The 9 cm transitions inside the Λ-doublet of the CH rotational ground state are found to be inverted over a wide range of physical conditions, which indicates the existence of some simple generalized population inversion mechanism. This mechanism seems to be a pumping cycle initiated by parity selective collisions to the first rotational level (Elitzur 1977).

Collisions with H favor the $^2\Pi_{1/2}$ $J = 1/2^+ \rightarrow J = 3/2^+$ transition with respect to the $1/2^- \rightarrow 3/2^-$ one (Bertojo, Cheung, and Townes 1976; Elitzur 1977; Dixon and Field 1979*a*, *b*). Such an agreement between authors does not exist in the case of H_2. Bertojo *et al.* found the same selectivity as for collisions with H atoms, whereas Dixon and Field suggest that the $- \rightarrow -$ collisions are favored (this would lead to an anti-inversion in the 9 cm lines). However, the cross section calculations seem to be less reliable in the case of H_2, where the reduced mass is larger and the potentials are harder than in the H case. In any case, for the slightly anisotropic interaction with H_2, inelastic cross sections would be lower than for H by perhaps one order of magnitude.

On the other hand, observations show the 9 cm lines to be inverted in quite dense clouds, where most of the hydrogen is thought to be in molecular form. This suggests in fact that all collisional processes favor the $+ \rightarrow +$ transition even in this medium.

In conclusion, a parity discrimination in the collisions favoring the $^2\Pi_{1/2}$ $J = 1/2^+ \rightarrow J = 3/2^+$ transition with respect to $^2\Pi_{1/2}$ $J = 1/2^- \rightarrow J = 3/2^-$ seems probable, although large uncertainties are still present. In the statistical equilibrium calculations, a unique set of collisional rates will be used, without regard to possible differences in the chemical composition of the clouds. Taking into account considerations of the above-mentioned authors, a 20% selectivity favoring $^2\Pi_{1/2}$ $J = 1/2^+ \rightarrow J = 3/2^+$ will be assumed. No other parity selection effect is considered.

Another important factor in collisions is the ratio between collisions joining different rotational states and those joining the sublevels inside a given rotational state ($C_{\Delta J \neq 0}/C_{\Delta J = 0}$). No calculations of this ratio has been achieved, but Dewangan and Flower (1982) have found that de-excitation to the rotational ground state of OH by collisions with H_2 can be about 3 times smaller than transitions inside the ground-state Λ-doublet. In this study $C_{\Delta J \neq 0}/C_{\Delta J = 0} = 0.3$ is assumed, but this factor will be considered almost like a free parameter in the calculations. To establish the collisional law, this ratio and the parity discrimination mentioned above were taken. De-excitations were assumed to be proportional to the statistical weight of the lowest level, and for the total cross section, the value 2×10^{-15} cm^{-2} was taken.

The collisional models considered until now do not provide preferential excitation of hyperfine levels. Differences observed in the excitation of hyperfine levels will be explained in the present work by means of a radiative mechanism. Of course, we cannot exclude the possibility of hyperfine asymmetries due to a particular collisional law, but even a hyperfine level selectivity in the collisional excitation $^2\Pi_{1/2}$ $J = 1/2 \rightarrow J = 3/2$ is not enough to explain the observations; this selectivity would have to be parity dependent (see § III*a*), and such a collisional law seems to be too ad hoc. Nevertheless, it would be interesting to study carefully the possibility of selection effects in collisional rates (see, e.g., Varshalovich and Khersonsky 1977).

Collisions with charged particles are not considered in the calculations. In fact, the rotational transitions due to collisions

with electrons or ions are quite improbable (Rogers and Barrett 1968; Goss and Field 1968; Bouloy and Omont 1977). Moreover, they closely follow a dipolar law ($+ \leftrightarrow -$ selection rule) which is inefficient in inducing anomalies in 9 cm line excitation. Therefore, the inclusion of charged particles would just contribute to microwave-line thermalization, which is essentially equivalent to a decrease in the parameter $C_{\Delta J \neq 0}/C_{\Delta J = 0}$.

III. EXCITATION MODELS

In order to test the efficiency of the different excitation processes, it is necessary to construct numerical excitation models. Here two kinds of models will be used. The first one consists of an "exact" treatment of transfer for a given cloud configuration, involving the radiative coupling between the different parts in the cloud. The numerical code used is very similar to the Monte Carlo program developed by Bernes (1978, 1979), which has been adapted in this study to the CH molecule. The second model is the well-known LVG, or Sobolev, approximation, in which radiative coupling is localized by assuming the existence of a large velocity gradient, greatly simplifying the problem and its interpretation. In most cases, LVG results are significant enough for understanding the excitation. Only when we want to study an intrinsically nonlocal effect is it necessary to consider an exact treatment.

a) Isotropic LVG Model

The Sobolev approximation consists essentially in introducing two escape probabilities, β and β_c, that enter into the spontaneous decay rate and radiative excitation rate, respectively, by multiplying the Einstein A-coefficient.

For a given transition $u \rightarrow l$ (see Castor 1970),

$$\dot{x}_u = -A\beta x_u + A\beta_c I_c(x_l - x_u) , \quad (1)$$

where x is the population per magnetic sublevel, $x = n/g$; I_c is the intensity at the $u \rightarrow l$ frequency emitted by a continuum source occupying a solid angle Ω_s; and

$$\beta = \int_0^1 d(\cos\theta)[1 - \exp(-\tau)]/\tau \; ; \quad (2)$$

$$\beta_c = (1/\Omega_s) \int_{\Omega_s} d(\Omega_s)[1 - \exp(-\tau)]/\tau \; . \quad (3)$$

In a radial velocity field, the opacity τ in a certain direction forming an angle θ with the radius vector is given at a distance r from the center by

$$\tau(\theta, r) = \tau_0/[1 + (\epsilon - 1)\cos^2\theta] ,$$
$$\epsilon = d \ln V(r)/d \ln r , \quad (4)$$
$$\tau_0 = \frac{c^3 A_{ul}}{8\pi\nu^3} g_u(x_l - x_u) \frac{r}{V(r)} .$$

In the simplest case, $V(r) \propto r$, $\epsilon = 1$, and τ does not depend on the angle. This is the isotropic LVG model to be considered in this subsection.

Calculations corresponding to an optically thin case, in the absence of infrared sources and physical conditions expected to be typical of interstellar clouds (see legend to Fig. 2*a*), are shown in Figure 2*a*. The introduction of a significant parity discrimination (20%) in collisions leads, as expected, to the inversion of the whole Λ-doublet, and no significant hyperfine anomaly is found.

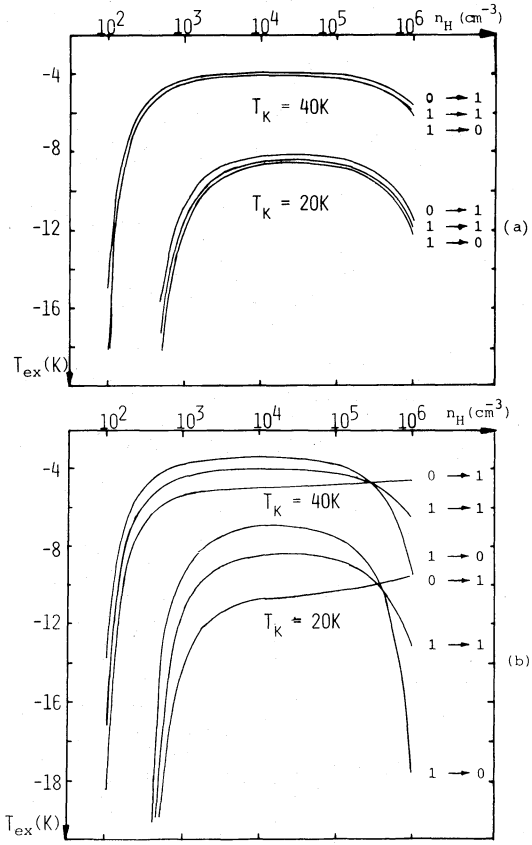

FIG. 2.—Excitation temperatures of CH 9 cm lines as functions of total density, n_H (cm^{-3}), in the absence of infrared sources. Physical conditions are kinetic temperature, T_K = 20 K, 40 K; logarithmic velocity gradient, $\epsilon = 1$; and column density to line width ratio: (*a*) in the optically thin case $N_{CH}/\Delta V = 2.5 \times 10^{11}$ cm^{-2} (km s^{-1})$^{-1}$; (*b*) in the optically thick case $N_{CH}/\Delta V = 2.5 \times 10^{13}$ cm^{-2} (km s^{-1})$^{-1}$.

When opacities of rotational transitions, τ_{IR}, are no longer negligible, the effects of trapping are perceived (Fig. 2*b*). When $\tau_{IR} \gg 1$, then β, $\beta_c \approx 1/\tau_{IR}$, and the radiative probabilities become proportional to $1/g_u$. If the population rates of the $J = 3/2$ levels are proportional approximately to their statistical weights, as they are for the collisional law taken here, a simple counting of possible decay probabilities shows that the $J = 1/2$ $F = 1$ levels are overpopulated with respect to the $F = 0$ ones. These effects persist when τ_{IR} is of the order of unity, as for the conditions in Figure 2*b*.

In these figures it can be noted that for very high densities ($n_H > 10^6$) the situation is inverted, $|T_{ex}(0 \rightarrow 1)| < |T_{ex}(1 \rightarrow 0)|$. The explanation is as follows: the presence of a certain opacity decreases the actual decay probability ($\beta < 1$), mainly for the most opaque component of $J = 3/2 \rightarrow 1/2$, i.e., $F = 2 \rightarrow 1$. At these high densities, collisional de-excitations start being competitive with radiative ones, causing more of a relative decrease in $2 \rightarrow 1$ radiative decay. The partial replacement of the $2 \rightarrow 1$ transition by $2 \rightarrow 1$ and $2 \rightarrow 0$ collisional transitions leads to a relative overpopulation of $F = 0$ levels. However, this mechanism, efficient only at such high densities, cannot explain the generalized $0 \rightarrow 1$ overexcitation.

As a test, calculations were also carried out taking a certain collisional hyperfine selectivity into account. In particular, the $\Delta J = 0$ $F = 1 \rightarrow 1$ collisions were considered to be more frequent than those in the preceding law by a factor of the same

order as the parity discrimination. As expected, numerical results show a larger excitation for the $0 \rightarrow 1$ transition; however, the method of obtaining this result seems too artificial because of the lack of facts about hyperfine collisional selectivity.

Moreover, $|T_{ex}(1 \rightarrow 0)| > |T_{ex}(1 \rightarrow 1)|$ was found, whereas observations show (Rydbeck *et al.* 1976; Whiteoak, Gardner, and Sinclair 1978) that both satellite lines are often more inverted than the main line. The only way to overcome this difficulty would be to assume that hyperfine selectivity depends on the parity.

In the calculations presented above, the presence of possible far-infrared sources is not considered. However, they are included in the results depicted in Figure 3 (*solid lines*), which are to be compared with those on the same figure (*dashed lines*) where the presence of IR sources is not involved. In these calculations, IR radiation should be due to dust emission. In this case,

$$I_c = W(\lambda) \frac{1}{\exp(h\nu/kT_D) - 1},$$

where T_D is the dust temperature, and W is essentially equal to its opacity $\propto \lambda^{-2}$ (see, e.g., Guibert, Elitzur, and Nguyen-Q-Rieu 1978). Note that, for this isotropic model, no difference in excitation is expected if one considers a discrete IR source instead of dust. It is easily shown that radiative decay following radiative excitation between two states cannot produce any anomaly, since excitation follows the same $1/\tau$ law as emission and therefore has the same effect, with the opposite sign. On the other hand, infrared absorption by $^2\Pi_{1/2}\, J = 1/2 \rightarrow {}^2\Pi_{3/2}\, J = 3/2$ initiates the following three-level cycle:

$$^2\Pi_{1/2}\, J = 1/2 \rightarrow {}^2\Pi_{3/2}\, J = 3/2$$
$$\rightarrow {}^2\Pi_{1/2}\, J = 3/2 \rightarrow {}^2\Pi_{1/2}\, J = 1/2\,,$$

which, in the presence of trapping in the $J = 3/2 \rightarrow J = 1/2$ transitions, induces the same kind of anomalies as those found in the collisional pumping case. (This cycle also produces a decrease in the excitation of the whole Λ-doublet, since it can interchange molecules between different parity levels, mixing the populations inside the rotational ground state.)

It can thus be concluded that this simple LVG approximation cannot explain the observed hyperfine anomalies; other processes must be taken into account in more complicated excitation models.

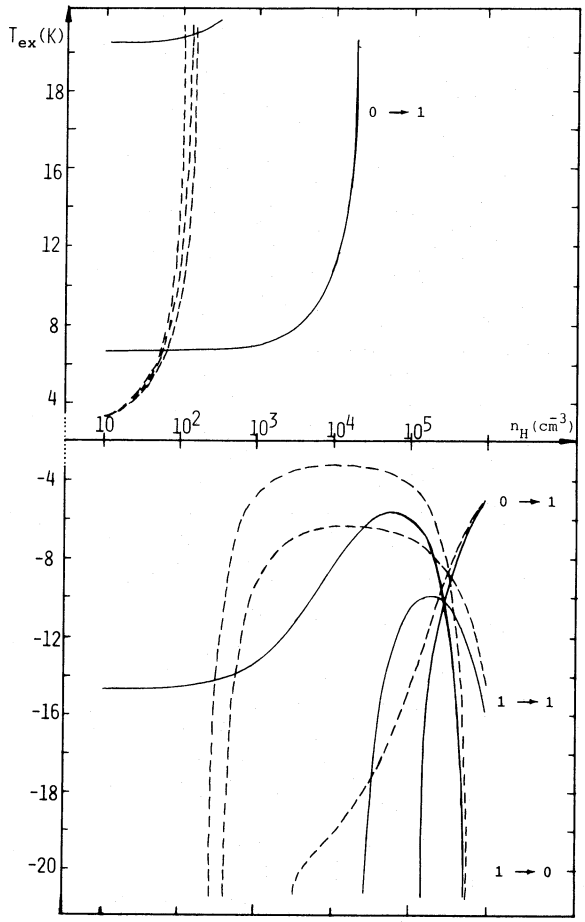

FIG. 3.—Excitation temperatures calculated when IR sources are considered (*solid lines*), with $T_K = 20$ K, $\epsilon = 1$, $N_{CH}/\Delta V = 7.5 \times 10^{13}$ cm^{-2} (km s^{-1})$^{-1}$, temperatures and opacity (at 80 μm) of the dust, $T_D = 20$ K and $W = 0.1$, respectively. Dashed lines represent the excitation temperatures obtained when IR sources are not taken into account but the other physical parameters are the same.

b) *The Effect of IR Radiation on Anisotropic LVG Models*

A more complicated model, which could account for the observed anomalies, is the one considered in this subsection. In this LVG model the existence of an IR source in the center of the cloud and a more complicated velocity field will be assumed.

Under certain physical conditions, the presence of a central source and the assumption that the cloud is in radial expansion with the nontrivial velocity field $V(r) \propto r^{\epsilon}$, $0 < \epsilon < 1$, gave rise to some drastic changes in the CH molecular excitation (numerical calculations are presented in Fig. 4). When infrared pumping is high enough (as compared with collisional pumping) to be the principal factor of excitation, the presence of the velocity field brings about a strong inversion of the $0 \rightarrow 1$ line, and even an anti-inversion of the $1 \rightarrow 0$ line. The calculations made in this study indicate that the main line temperature is often between the other two. As can be seen in § III*a*, these are not satisfactory results, when compared with observations.

This peculiar excitation can be easily explained by the opacity behavior shown in equation (4). When the logarithmic velocity gradient ϵ is smaller than unity, the dependence of τ on the angle θ shows that the opacity reaches its maximum in the radial direction and decreases for other escape directions; in these calculations $\epsilon = 0.25$, and τ is 4 times greater in the radial direction than in the perpendicular one. This directional trapping mainly affects the rotational transitions, which are the thickest ones. It is clear that radiative decay from $J = 3/2$ levels does not follow the same law as radiative excitation. While the absorption rates of radiation coming from the central source follow the $1/g_u$ law corresponding to an optically thick case for a relatively wide range of opacities, the emission rates do not. This generates an overpopulation of the $F = 0$ levels with respect to the $F = 1$ ones, by a mechanism acting inversely to that responsible for collisional overexcitation of the $1 \rightarrow 0$ transition. For column densities that are much higher than those taken here, this effect disappears since emission can also be considered as optically thick. For the two rates

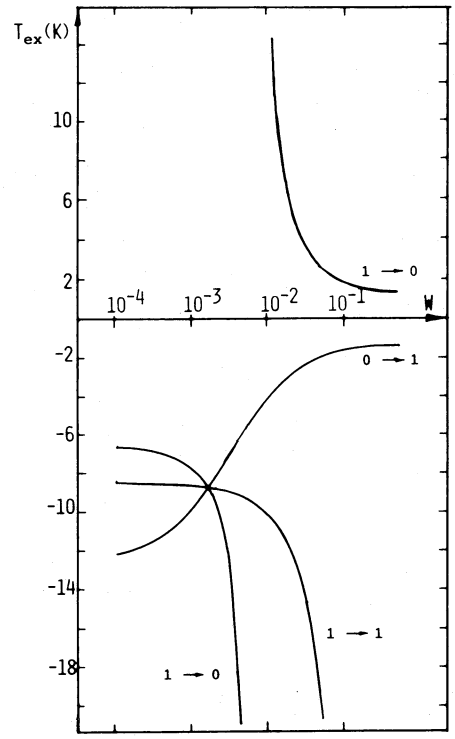

FIG. 4.—Excitation temperatures of CH radio lines as functions of the dust opacity (at 80 μm), W, calculated when a central IR source and a nontrivial velocity field are considered, with physical conditions: $T_K = 20$ K, $n_H = 1 \times 10^4$ cm^{-3}, $\epsilon = 0.25$, $N_{CH}/\Delta V = 2.5 \times 10^{13}$ cm^{-2} (km s^{-1})$^{-1}$, and $T_D = 20$ K.

following the same law, the system's behavior is similar to that in the preceding subsection when $\epsilon = 1$.

Although this model explains the $0 \rightarrow 1$ line's greatest inversion, it is not satisfactory for two reasons: (1) the $1 \rightarrow 1$ line is more inverted than the $1 \rightarrow 0$ one, which, as stated before, is not generally observed, and (2) it is too particular a model to explain the generalized hyperfine asymmetries (there is no experimental evidence of such velocity fields, and the central infrared source does not always exist, e.g., Cas A).

c) *Nonlocal Excitation Models*

The model developed in the preceding subsection presents serious drawbacks. However, the results obtained suggest the possibility of reaching satisfactory excitation conditions in the presence of central IR sources. Nonlocal absorption of their emission could cause different behaviors for the different hyperfine components of the $J = 1/2 \rightarrow J = 3/2$ transition, the infrared intensity available for the strongest components being weaker (as in the model developed by Litvak 1969 for OH), and thus able to modify the satellite 9 cm lines in a suitable manner. The result of taking into account the influence of all processes and the contributions from all parts in the cloud can only be studied using a nonlocal "exact" treatment of radiative transfer.

The Monte Carlo numerical code developed by Bernes (1978, 1979) was used; the cloud models were chosen to correspond to the geometry (spherical) and physical conditions characteristic of clouds associated with H II regions. The conclusions extracted from the results are given here; the details of the numerical treatment, the physical model parameters, and the quantitative results themselves can be found in the Appendix.

When compared with LVG models, neither homogeneous nor inhomogeneous cloud models, in the absence of central IR sources, lead to essentially new results, except for showing the expected modification in excitation toward the edges (Figs. 6*a*–6*b*).

Strong modifications in the excitation, with respect to the preceding case, were produced in the presence of a central infrared source. However, when no macroscopic velocity field is introduced (Figs. 7*a*–7*b*), the general trend of satellite-line anomalies, $|T_{ex}(1 \rightarrow 0)| < |T_{ex}(1 \rightarrow 1)| < |T_{ex}(0 \rightarrow 1)|$, did not change. It seems that (at least under the physical conditions expected for clouds associated with H II regions) the collisional mechanism and the purely radiative cycle $J = 1/2 \rightarrow {}^2\Pi_{3/2}$ $J = 3/2 \rightarrow {}^2\Pi_{1/2}$ $J = 3/2 \rightarrow J = 1/2$ are more efficient in the reinforcement of the $1 \rightarrow 0$ excitation than the anticipated nonlocal phenomenon of Litvak, which in principle is able to overexcite the $0 \rightarrow 1$ transition. Note in the numerical results the important effects near the boundaries of equal-density regions.

The introduction of a macroscopic field of the same type as those presented in § III*b* leads, as expected, to a slight overexcitation of the $0 \rightarrow 1$ transition (Fig. 8). In the calculations the microscopic velocity dispersion was taken to be only 4 times smaller than the total macroscopic dispersion, since otherwise, predicted spectrum shapes would vary strongly depending on the observed direction inside the cloud, which is not the case. Consequently, the $0 \rightarrow 1$ anomaly is not as strong as that found above when using an LVG approximation, which implicitly assumes that macroscopic velocities are much larger than microscopic ones.

Thus, the same effects found by means of LVG models are reproduced in the exact treatment and overcome possible nonlocal particularities. Once again, $0 \rightarrow 1$ overexcitation is only obtained for physical conditions which are too restricted, and in this case, $1 \rightarrow 0$ is underexcited. It can be concluded that a substantial modification in the classical treatment of the problem seems necessary to explain the observed anomalies.

d) *Rotational Line Overlap*

The overlap of two lines due to their Doppler width implies important modifications of radiative transfer and, therefore, of statistical equilibrium equations. The possibility of changes in CH excitation due to line overlap was previously suggested by Zuckerman and Turner (1975) and Elitzur (1977), who emphasized the need of a detailed investigation. We will present in this subsection a systematic study and numerical calculations concerning this effect, which will prove to be the best candidate for explaining 9 cm anomalies. Energy separation of the ${}^2\Pi_{1/2}$ $J = 3/2$ sublevels is not well known, but it seems clear that the two lowest (parity +) hyperfine levels are very close. Levy and Hinze (1975) found that $E(2^+)$–$E(1^+)$ lies between -1 MHz and $+16$ MHz. For the ${}^2\Pi_{1/2}$ $J = 3/2 \rightarrow {}^2\Pi_{1/2}$ $J = 1/2$ frequency, a line width of 6 km s^{-1} (often observed) corresponds to 10 MHz, and therefore, an almost total or, at least, partial overlap of transitions ${}^2\Pi_{1/2}$ $J = 3/2(F = 2^+) \rightarrow J = 1/2(F = 1^-)$ and ${}^2\Pi_{1/2}$ $J = 3/2(F = 1^+) \rightarrow J = 1/2(F = 1^-)$ is very probable. However, it must be noted that, as long as values of these parameters are not sure, the very possibility of line overlap remains somewhat uncertain. Another possible overlap is the one due to the weak hyperfine splitting in the upper Λ-doublet of the ${}^2\Pi_{1/2}$ $J = 3/2$ state; however, from calculations by Levy and Hinze, this splitting is on the average

about twice as large as in the lower Λ sublevel. Instead of complicating the discussion with considerations about the relative intensity of the two effects, this second overlap will be ignored. Anyway, the effect of both will be shown to be very similar. No other overlapping seems possible according to the Levy and Hinze results.

The most important consequence of line overlap is the significant enhancement of trapping in the overlapped lines (e.g., Bujarrabal and Nguyen-Q-Rieu 1980). Consequently, line overlap produces a decrease in radiative rates of the transitions involved. For the $2^+ \rightarrow 1^-$ rotational transition case, a larger trapping has no effect on the 9 cm line excitation, since this rotational transition is the only efficient de-excitation from the $^2\Pi_{1/2}$ $J = 3/2(F = 2^+)$ level, and molecules in this level are compelled to leave it in this way. However, in the $1^+ \rightarrow 1^-$ transition case, an increase in trapping signifies that molecules will leave the $^2\Pi_{1/2}$ $J = 3/2(F = 1^+)$ level relatively more frequently through the $1^+ \rightarrow 0^-$ rotational component. Note that $1^+ \rightarrow 1^-$ component is the weakest one, and therefore, it is also relatively sensitive to overlap. For example, if its "original" opacity is $\tau_{1\rightarrow 1} \approx 0.1$, when overlap is present, the "effective" opacity is $\tau_{1\rightarrow 1} + \tau_{2\rightarrow 1} \approx 0.6$. For this range of opacity, trapping is already efficient enough to explain the observed differences in T_{ex}, since, for the 9 cm line ($h\nu/k = 0.16$ K), an increase of excitation from $T_{ex} = -16$ K to $T_{ex} = -8$ K in a component just requires a very weak increase in the corresponding upper level population (of $\sim 1\%$). The overlap effect, of course, disappears for very small rotational-line opacities. Whether the $^2\Pi_{1/2}$ $J = 3/2$ is populated by collisions from the ground state or by radiative cascades from $^2\Pi_{3/2}$ $J = 3/2$, this trend favoring the $^2\Pi_{1/2}$ $J = 3/2(F = 1^+) \rightarrow {}^2\Pi_{1/2}$ $J = 1/2(F = 0^-)$ component gives rise to a neat molecule flux from $J = 1/2(F = 1^-)$ to $J = 1/2(F = 0^-)$. The overpopulation of the 0^- level leads to an overexcitation of the $0^- \rightarrow 1^+$ transition relative to the other 9 cm lines. (The other less probable overlap would produce an underpopulation of the 1^+ levels, with similar consequences in excitation.)

Calculations involving line overlap confirm the above predictions about its effect on the excitation of 9 cm lines. Line overlap has been numerically treated using the simplified method described by Bujarrabal and Nguyen-Q-Rieu (1980) since lack of knowledge about level energies prevents more detailed calculations. Note that in this treatment the overlap is supposed to be total; therefore, the effect would be somewhat overestimated for sources of small velocity dispersion. Results are presented in Figures 5*a* and 5*b* for the same physical conditions considered in previous subsections (also included is a case with $C_{\Delta J\neq 0}/C_{\Delta J=0} = 0.2$; see § II). Together with a net overexcitation of the $0 \rightarrow 1$ line, it can be observed that the $1 \rightarrow 0$ transition is slightly more excited than the main line, as a consequence of the general mechanism explained in § III*a*.

These numerical results are in good agreement with the general observational characteristics of CH microwave lines. In view of this agreement and the apparent generality of the mechanism, we believe that line overlap very probably operates in the CH case and is the origin of hyperfine anomalies observed in interstellar clouds.

IV. CONCLUSION

The main characteristics of the excitation of the CH 9 cm lines have been discussed. The generalized inversion of the three CH lines has already been explained (e.g., Elitzur 1977) as a consequence of parity discrimination in collisions from the rotational ground state to the first excited one. This point has been discussed in considering more recent calculations by Dixon and Field, and we confirm the possibility of a collisional pumping for the CH weak masers.

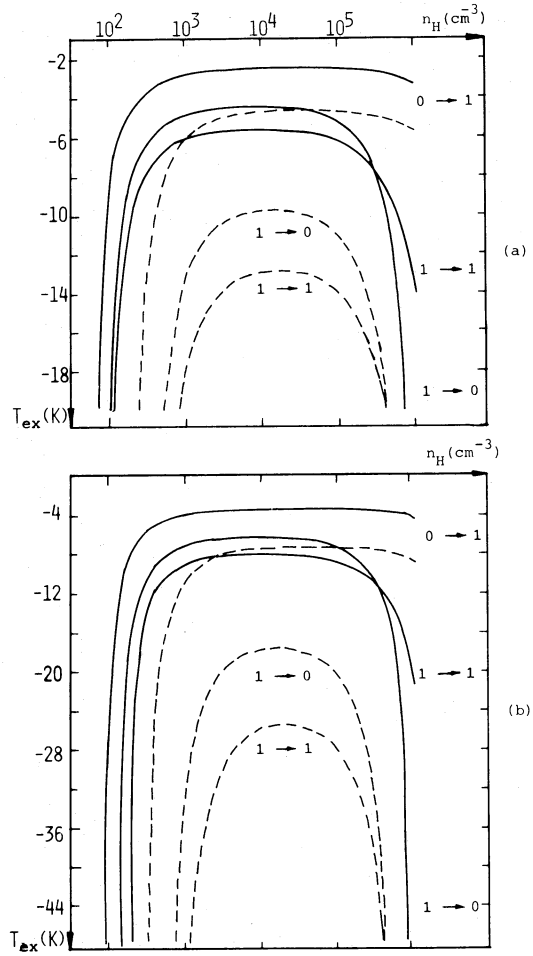

FIG. 5.—Excitation temperatures calculated in the presence of rotational line overlap (see § III) with the same physical conditions as in Fig. 2. Fig. 5*b* demonstrates the effects of changing the collisional parameter to $C_{\Delta J\neq 0}/C_{\Delta J=0} = 0.2$. *Solid lines*, $T_K = 40$ K; *dashed lines*, $T_K = 20$ K.

Another important characteristic of CH excitation is the very widespread overexcitation of the $0 \rightarrow 1$ satellite line. Simple LVG models are unable to explain this phenomenon; in fact, they predict an underexcitation of this line. Classical models (i.e., models which do not take line overlap into account) can explain this excitation anomaly only by postulating the presence of a central IR source and certain particular velocity fields. In this case, the other two lines present a predicted excitation trend ($1 \rightarrow 1$ more excited than $1 \rightarrow 0$) contradictory to observations. The possibility of nonlocal effects being important was tested by means of an "exact" treatment of radiative transfer, but the results were also negative.

Finally, agreement between observational and theoretical results was obtained only by including the effects of line overlap in the model. Although rotational frequencies of CH are not very well known, it seems that the components $F = 2^+ \rightarrow 1^-$, $F = 1^+ \rightarrow 1^-$ of the $^2\Pi_{1/2}$ $J = 3/2 \rightarrow J = 1/2$ rotational transition overlap at least partially, for the usual velocity dispersions. This leads to an overpopulation of the 0^-

level and consequently to an overexcitation of the $0 \rightarrow 1$ line, in agreement with observations. The predicted excitation of the other transitions also agrees with apparent observational trends. Therefore, we believe that the excitation anomalies of CH 9 cm lines are very probably a consequence of the overlap of the above-mentioned rotational components.

The main drawback of the mechanism involving line overlap is our inadequate knowledge of the energy level separation. This problem prevents a very detailed treatment of overlap and even casts some doubt on its possibility. We could, on the other hand, construct models including particular collision laws able to explain excitation anomalies. However, these collisional laws would have to be too ad hoc, and no indication exists of such a collision behavior (§ II); meanwhile, the best available data on level structure strongly suggest the existence of line overlap.

APPENDIX

Nonlocal excitation models have been analyzed by means of the Monte Carlo numerical method developed by Bernes (1978, 1979). The cloud model is a spherical region which is divided into 15 spherical concentric shells, each one with a

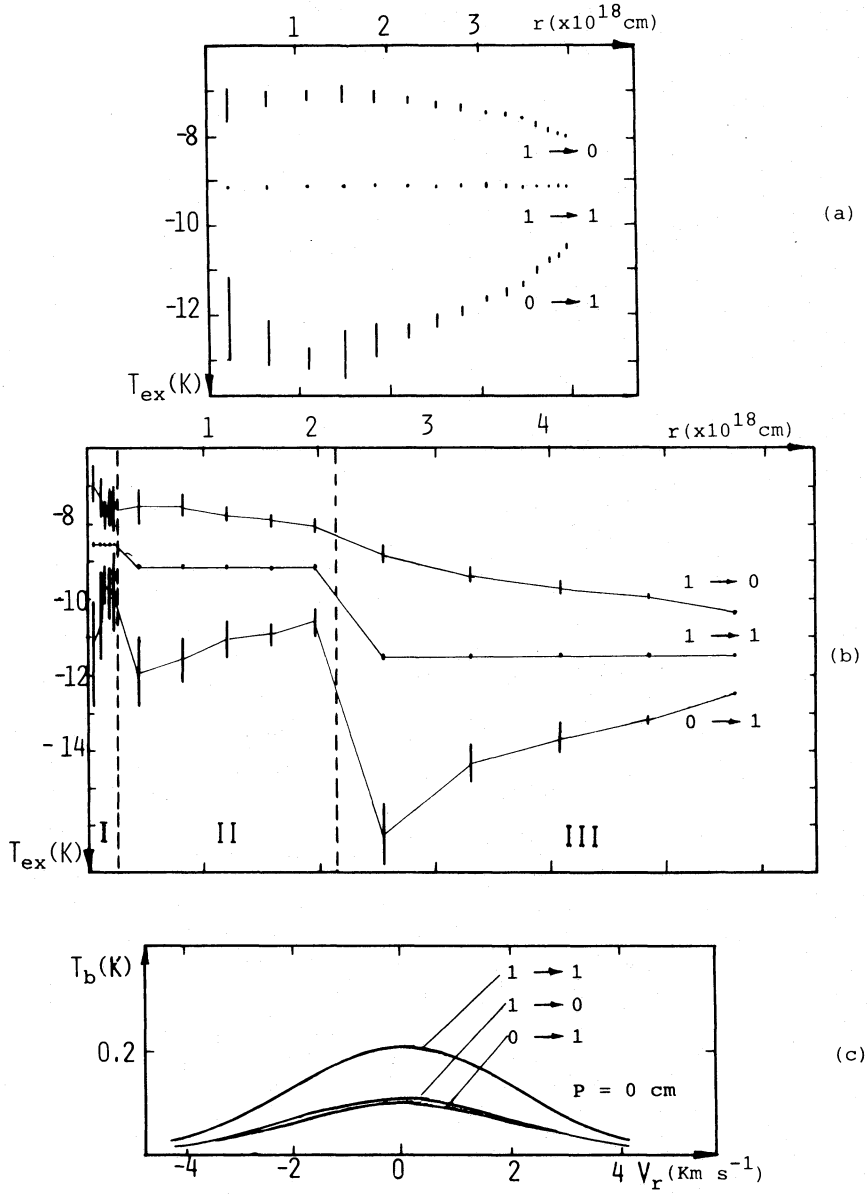

FIG. 6.—Excitation temperatures as functions of the distance r from the cloud center (note the different scales in figures) calculated in the absence of a central IR source and a macroscopic velocity field using (*a*) a homogeneous, (*b*) an inhomogeneous cloud model. Physical conditions for each model are given in the text. Temperatures are represented at positions halfway between the inner and outer radii of each shell. Fig. 6*c* shows the profiles of CH 9 cm lines numerically obtained (with impact parameter $p = 0$ cm) in the inhomogeneous case; brightness temperatures are plotted as a function of the radial velocity relative to the cloud center. Error bars show the standard deviations where they are large enough to be plotted.

kinetic temperature, a microscopic velocity dispersion, and a total density (in our models all the shells have the same kinetic temperature and microscopic velocity dispersion). Their values will be stated later for the different cases. All the physical conditions used here have been chosen to account for the supposed physical parameters of clouds associated with H II regions. The ratio between the CH density and the total density has been chosen to be 1×10^{-8}. In the analysis, we included the levels represented in Figure 1 with all the possible radiative transitions between them except the radio lines corresponding to the excited rotational states; therefore, 23 CH radiative transitions have been taken into account.

In spite of the well-known advantages of the Monte Carlo method, one drawback is the important calculation noise inherent in the use of random numbers. This is especially noticeable in the case of long-wavelength transitions (such as CH microwave lines), for which very small errors in level populations can induce large dispersions in excitation temperatures. A great computational effort has been made in order to obtain convergence from initial populations and to reduce the noise to reasonable limits. Once the convergence achieved in the calculations for excitation temperatures was considered to be satisfactory, a set of runs consisting of 20 iterations was also made with different random numbers in order to stabilize and diminish the noise level. It can be seen in the figures that the calculation noise is still appreciable in $0 \rightarrow 1$ and $1 \rightarrow 0$ transitions for the most inner shells; in $1 \rightarrow 1$ the noise level is always negligible.

Each one of the 20 iterations of the runs consists of 1000 model photons, representing in the numerical treatment the photons emitted in the CH transitions and those coming from the 2.7 background radiation or from a central IR source (if it should be present). Model photons are distributed over bands, each one covering a CH line; they are numerically followed in their travel through the cloud.

A sample of the different models analyzed is presented below; the results from this sample are depicted in Figures 6–8, in which the mean excitation temperatures obtained for the CH 9 cm lines and the line profiles predicted by some of these models are plotted.

I. SIMPLE CLOUD MODELS

Two models, one homogeneous and the other inhomogeneous, will be presented now. These models lack a central IR source and a macroscopic velocity field. Physical characteristics for the homogeneous cloud model (as well as for the other homogeneous models presented in this Appendix) are: radius, 4×10^{18} cm; total density, 3×10^{3} cm^{-3}; and kinetic temperature, 20 K. For this simplest model, the microscopic velocity dispersion is 3 km s^{-1}. In order to achieve a smaller noise level, the thickness of the shells is greater in the inner parts than in the outer parts of the cloud; moreover, the smaller size of the outer shells allows us to show possible boundary effects more clearly.

In the inhomogeneous cloud models the cloud is divided into three concentric regions (I, II, III in figures), each one subdivided into five shells of equal thickness, with total densities 1×10^{4} cm^{-3}, 3×10^{3} cm^{-3}, and 1×10^{3} cm^{-3}. The radius of the cloud is 6×10^{18} cm, and the thickness of each region, increasing toward the surface, has been chosen so that the column density of the clouds was 1.2×10^{14} cm^{-2}, the

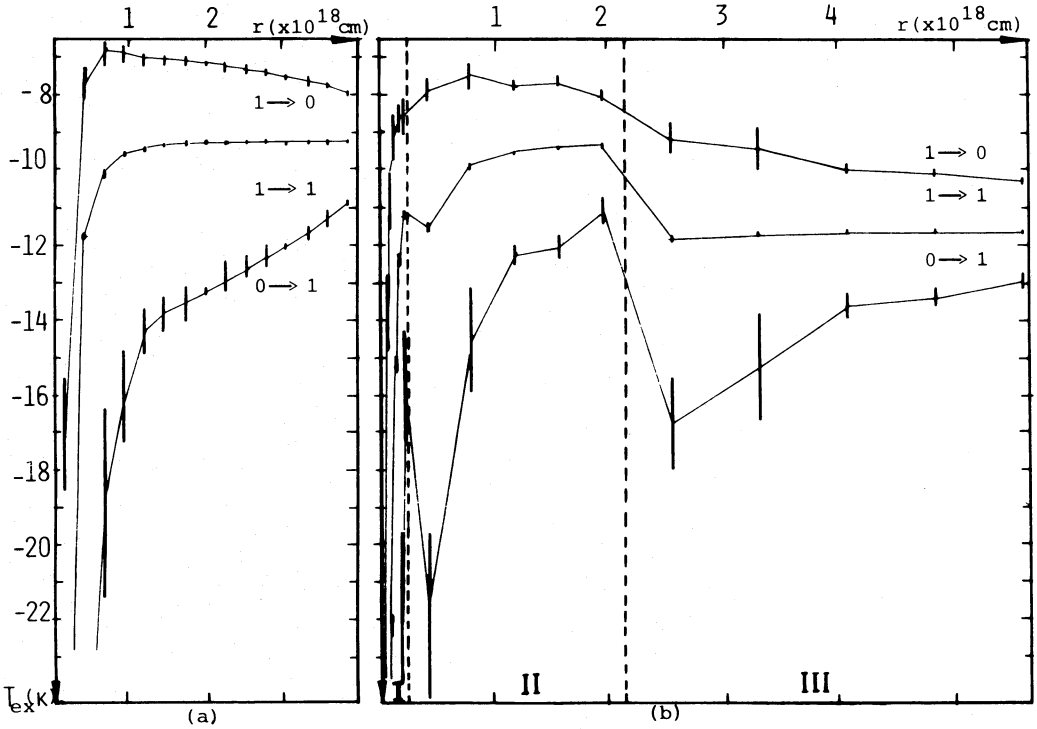

FIG. 7.—Excitation temperatures calculated when a central IR source is included in the calculations for (*a*) the homogeneous, (*b*) the inhomogeneous cloud.

same as in the homogeneous cloud models. The kinetic temperature is 20 K, and the microscopic velocity dispersion, 3 km s^{-1}.

Calculations depicted in Figures 6*a* (homogeneous) and 6*b* (inhomogeneous cloud) do not reveal any new results with respect to the equivalent LVG models, except some modification in the excitation near the edges (modification that is also present in all the models analyzed). In these regions photons emitted in $J = 3/2 \rightarrow 1/2$ transitions can escape from the cloud, and then a slight decrease of the rotational transition trapping is produced. Figure 6*c* shows line profiles of CH 9 cm lines predicted in calculations for the inhomogeneous model, in a direction defined by the impact parameter $p = 0$ cm; standard deviations in the numerical results are negligible.

II. MODELS WITH CENTRAL IR SOURCE

In these models, an IR source is assumed to be in the center of the cloud. For both homogeneous and inhomogeneous models the temperature of this IR source is 20 K and its radius is 6×10^{15} cm. The other physical parameters are the same as for the simple cloud models in the previous section. In the homogeneous case, all the shells have the same thickness since the noise is now less important, and then the size of the inner shells has no reason for being very small. Numerical results are shown in Figures 7*a* (homogeneous) and 7*b* (inhomogeneous cloud).

III. ANISOTROPIC NONLOCAL MODELS

In this model a homogeneous cloud is expanding with velocity

$$V(r) = V_M(r/R)^{\epsilon} ,$$

in which V_M, 2 km s^{-1}, is the velocity at the periphery, R is the radius of the cloud, and the logarithmic velocity gradient, ϵ, is taken to be 0.2. In the center of the cloud there is an IR source with the same characteristics as above. Density and kinetic temperature are the same as in the other homogeneous clouds,

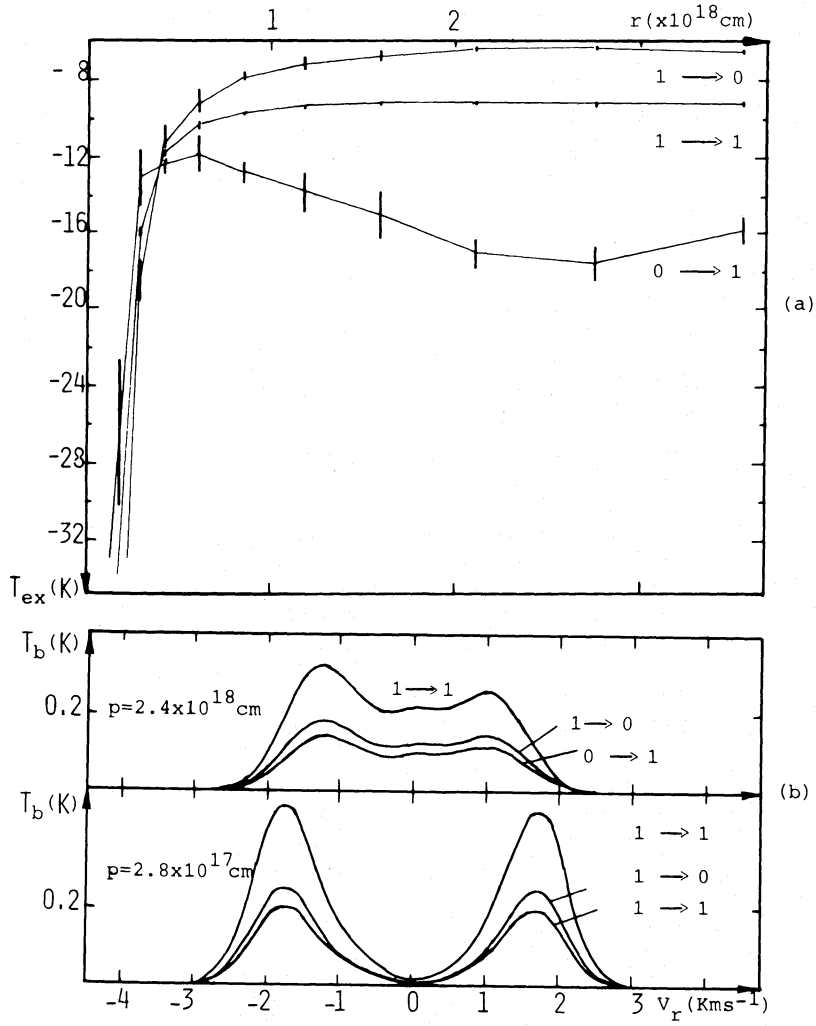

FIG. 8.—(*a*) This is similar to Fig. 7*a*, except that a macroscopic velocity field is included in the calculations (see text). (*b*) Profiles for CH 9 cm lines numerically obtained in this model for the two different impact parameters, *p*, indicated in the graphs.

3×10^3 cm^{-3} and 20 K. The microscopic velocity dispersion is 0.5 km s^{-1}.

The thickness of the shells is gradually increased toward the surface so that the change in the radial velocity between the inner and the outer radii of each shell is the same for all of them. This condition helps to assure that there is not a significant change in the opacity at any given frequency in the model photons' trajectory, and therefore, a reduction in the computation time is achieved. Figure 8*a* shows the excitation temperatures and standard deviations obtained for this model. Figure 8*b* shows the line profiles, predicted in this case, in directions defined by impact parameters 2.8×10^{17} cm and 2.4×10^{18} cm.

REFERENCES

Bernes, C. 1978, *Stockholm Obs. Rept.*, No. 15.
———. 1979, *Astr. Ap.*, **73**, 67.
Bertojo, M., Cheung, A. C., and Townes, C. H. 1976, *Ap. J.*, **208**, 914.
Bouloy, D., and Omont, A. 1977, *Astr. Ap.*, **61**, 405.
Bujarrabal, V., and Nguyen-Q-Rieu 1980, *Astr. Ap.*, **91**, 283.
Castor, J. I. 1970, *M.N.R.A.S.*, **149**, 111.
Dewangan, D. P., and Flower, D. R. 1982, *M.N.R.A.S.*, **199**, 457.
Dixon, R. N., and Field, D. 1979*a*, *Proc. Roy. Soc. London, A*, **368**, 99.
———. 1979*b*, *M.N.R.A.S.*, **189**, 583.
Elitzur, M. 1976, *Ap. J.*, **203**, 124.
———. 1977, *Ap. J.*, **281**, 677.
Goss, W. M., and Field, G. B. 1968, *Ap. J.*, **151**, 177.
Guibert, J., Elitzur, M., and Nguyen-Q-Rieu. 1978, *Astr. Ap.*, **66**, 195.
Levy, D. H., and Hinze, J. 1975, *Ap. J.*, **200**, 236.
Litvak, M. M. 1969, *Ap. J.*, **156**, 471.
Rogers, A. E. E., and Barrett, A. H. 1968, *Ap. J.*, **151**, 163.
Rydbeck, O. E. H., Kollberg, E., Hjalmarson, A., Sume, A., Elldér, J., and Irvine, W. M. 1976, *Ap. J. Suppl.*, **31**, 333.
Varshalovich, D. A., and Khersonsky, V. K. 1977, *Ap. Letters*, **18**, 167.
Whiteoak, J. B., Gardner, F. F., and Sinclair, M. W. 1978, *M.N.R.A.S.*, **184**, 235.
Zuckerman, B., and Turner, B. E. 1975, *Ap. J.*, **197**, 123.

VALENTIN BUJARRABAL and FRANCISCO SALINAS: Observatorio Astronómico Nacional, Centro Astronómico de YEBES, Apartado 148, Guadalajara, Spain

ISABEL GONZALO: Departamento de Optica y Estructura de la Materia, Facultad de Ciencias Físicas, Universidad Complutense, Madrid–3, Spain